Morphologically Controlled Synthesis of Hydroxyapatite with Partial Substitution of Fluorine

Hui Gang Zhang, Qingshan Zhu,* and Yong Wang

Multiphase Reaction Laboratory, Institute of Process Engineering, Chinese Academy of Sciences, P.O. Box 353, Beijing 100080, China

Received June 23, 2005. Revised Manuscript Received August 6, 2005

Morphologies of hydroxyapatite with partial substitution of fluorine (FHAp) have been finely modulated from prickly spheres, whisk brooms, flowers, dandelions, and nanofibers to ultralong nanoribbons through altering the reaction conditions and adding glutamic acid. X-ray diffraction, high-resolution transmission electron microscopy, energy-dispersive X-ray spectroscopy, and so forth were performed for characterizing the resultant powders and analyzing the growth process. Condition experiments were compared comprehensively and revealed that FHAp crystals with various morphologies were formed, generally, through a fractal growth process of double splitting.

Introduction

Systematically manipulating the morphology and architecture of inorganic crystals in microscale and nanoscale levels is a significant challenge, which attracts increasing attention because of their strong influence on material properties.[1−3] For example, in the biomineralization process of vertebrate hard tissues, some specific molecules control the nucleation and growth of inorganic crystals (hydroxyapatite, HAp, $Ca_{10}(PO_4)_6(OH)_2$), resulting in the formation of hierarchical structure of teeth and bones with superior mechanical properties.[4,5] Thus, controlled syntheses of apatitic crystals with various morphologies have been the focus of intensive research out of the desire to more completely understand the biomineralization and utility in industrial and biomedical applications.[6] Inspired by the biomineralization, the molecular manipulation of inorganic crystals with organic growth modifiers gradually develops into a powerful tool for the design of novel materials.[7] Actually, a variety of organic molecules, such as hexadecyltrimethylammonium bromide, sodium dodecyl sulfate, amino acids, protein, monosaccharide, and so forth, have been used to synthesize hydroxyapatite with fibrous and flakelike morphologies.[8−13] However, the mineral phase in vertebrate calcified hard tissues is not pure stoichiometric hydroxyapatite but is partially substituted by some foreign ions, such as F^-, CO_3^{2-}, Na^+, and some organic molecules, which endue the mineral phase with special properties.[14] Among them, of great importance is fluorine substitution, which enhances acid resistance and stability of hydroxyapatite.[15] Recent studies showed that the incorporation of fluorine into hydroxyapatite improved the mechanical properties of apatite ceramics[16] and induced better biological response.[17] Therefore, to mimic the biological apatite with special morphologies and to control morphological syntheses of fluorine-substituted hydroxyapatite (FHAp) crystals in microscale and nanoscale levels is of great value and urgently needed. However, so far there is no investigation on the controllable synthesis of FHAp with various morphologies.

Previous studies[18−20] showed that some amino acids could inhibit the growth of hydroxyapatite as a result of the adsorption on HAp crystal surfaces through electrostatic attraction and hydrogen bonds, which possibly influence the morphological development of apatite crystals. More importantly, it has been found that some glutamic acid (Glu)-rich proteins played a significant role in biomineralization of hard tissues[1,21−24] because of the interaction between carboxyl groups and calcium ions on the surfaces of HAp

* To whom correspondence should be addressed. Tel. and Fax: +86-10-62536108. E-mail address: qszhu@home.ipe.ac.cn.

(1) Hartgerink, J. D.; Beniash, E.; Stupp, S. I. *Science* **2001**, *294*, 1684.
(2) Yang, J.; Qi, L.; Zhang, D.; Ma, J.; Cheng, H. *Cryst. Growth Des.* **2004**, *4*, 1371.
(3) Ball, V.; Planeix, J. M.; Félix, O.; Hemmerlé, J.; Schaaf, P.; Hosseini, M. W.; Voegel, J. C. *Cryst. Growth Des.* **2002**, *2*, 489.
(4) Weiner, S.; Addadi, L. *J. Mater. Chem.* **1997**, *7*, 689.
(5) Fractzl, P.; Gupta, H. S.; Paschalis, E. P.; Roschger, P. *J. Mater. Chem.* **2004**, *14*, 2115.
(6) Murphy, W. L.; Mooney, D. J. *J. Am. Chem. Soc.* **2002**, *124*, 1910.
(7) Stupp, S. I.; Braun, P. V. *Science* **1997**, *277*, 1242.
(8) Cao, M.; Wang, Y.; Guo, C.; Qi, Y.; Hu, C. *Langmuir* **2004**, *20*, 4784.
(9) Walsh, D.; Kingston, J. L.; Heywood, B. R.; Mann, S. *J. Cryst. Growth* **1993**, *133*, 1.
(10) Donners, J. J. J. M.; Nolte, R. J. M.; Sommerdijk, N. A. J. M. *Adv. Mater.* **2003**, *15*, 313.
(11) Matsumoto, T.; Okazaki, M.; Inoue, M.; Hamada, Y.; Taira, M.; Takahashi, J. *Biomaterials* **2002**, *23*, 2241.
(12) Busch, S. *Angew. Chem., Int. Ed.* **2004**, *43*, 1428.
(13) Gonzalez-McQuire, R.; Chane-Ching, J. Y.; Vignaud, E.; Lebugle, A.; Mann, S. *J. Mater. Chem.* **2004**, *14*, 2277.
(14) Verbeeck, R. M. H.; De Maeyer, E. A. P.; Driessens, F. C. M. *Inorg. Chem.* **1995**, *34*, 2084.
(15) Busch. S.; Schwarz, U.; Kniep, R. *Chem. Mater.* **2001**, *13*, 3260.
(16) Gross, K. A.; Rodríguez-Lorenzo, L. M. *Biomaterials* **2004**, *25*, 1385.
(17) Dhert, W. J. A.; Klein, C. P. A. T.; Jansen, J. A.; Van der Velde, E. A.; Vriesde, R. C.; Rozing, P. M.; De Groot, K. *J. Biomed. Mater. Res.* **1993**, *27*, 127.
(18) Bigi, A.; Boanini, E.; Bracci, B.; Falini, G.; Rubini, K. *J. Inorg. Biochem.* **1999**, *75*, 145.
(19) Spanos, N.; Klepetsanis, P. G.; Koutsoukos, P. G. *J. Colloid Interface Sci.* **2001**, *236*, 260.
(20) Chander, S.; Fuerstenau, D. W. Solubility and Interfacial Properties of Hydroxyapatite: a Review. In *Adsorption on and Surface Chemistry of Hydroxyapatite*; Misra, D. N., Eds.; Plenum Press: New York, 1982.
(21) Tsortos, A.; Nancollas, G. H. *J. Colloid Interface Sci.* **1999**, *209*, 109.

10.1021/cm051357a CCC: $30.25
Published on Web 10/18/2005

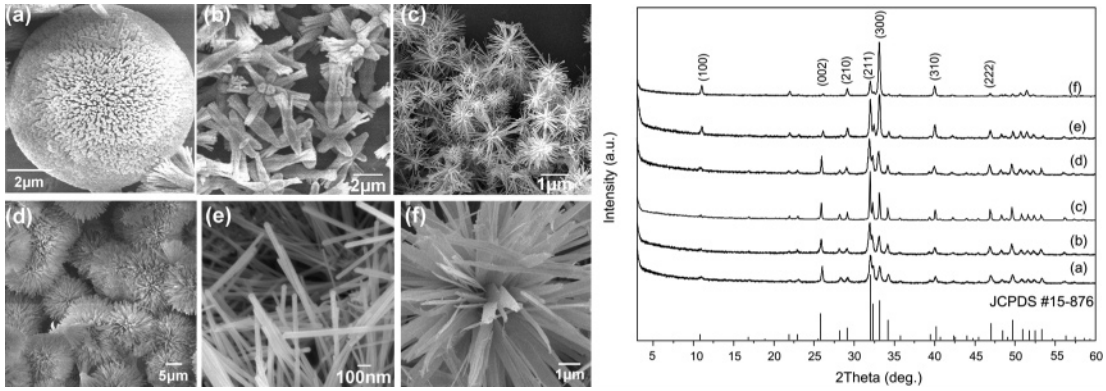

Figure 1. FESEM images and XRD patterns of the samples obtained under varied preparation parameters. (a) M2, $C_{Ca}/C_P/C_F$ =1.21:1.52:0.01; (b) M2, C_F = 0.02; (c) M1, C_g = 3.6, (d) M3, C_{OH} = 0.8; (e) M3, C_{OH}/T = 0.8:160; and (f) M3, $C_F/C_{OH}/T$ = 0:1.04:160.

Table 1. Preparation Parameters and Properties of Products[a,b]

model reaction	conditions		morphology
	T (°C)	$C_G/C_{Ca}/C_P/C_F/C_{OH}$ (g)	
M1	150	v:1.50:1.21:0.04:v	from aggregated nanospheroids to rayed nanorods
M2	150	3.6:1.50, v:1.21, v:v:0.06	from prickly spheres and whisk brooms to bundled FHAp rods
M3	150, v	3.6:1.43:1.21:0.03, v:v	from dandelion-like aggregates and nanofibers to nanoribbons

[a] C_G, C_{Ca}, C_P, C_F, and C_{OH} represent the added amounts of glutamic acid, calcium nitrate, dipotassium hydrogen phosphate, sodium fluoride, and potassium hydroxide, respectively. [b] v means that the parameter was varied in a specified experiment and will be given in the later sections.

crystals[25] and precursors.[1] Is there a possibility that the synthesis of FHAp is morphologically controlled by means of the influence of the basic and functional units of proteins, amino acid, in an in vitro system? If possible, it will not only produce FHAp with various morphologies but also provide an efficient method for mass production. Thus, the aim of this work is to investigate the influence of glutamic acid upon the formation of FHAp crystals and to realize the controllable syntheses of FHAp crystals with some novel morphologies in nanoscale and microscale levels.

Experimental Section

All chemicals (analytical grade) were purchased from Beijing Chemicals Corp., China, and used as received without further purification. The reagents used were weighted according to the model reactions in Table 1 with some modifications which were described in the later section. A typical procedure was performed as follows:

Glutamic acid and calcium nitrate [$Ca(NO_3)_2{\cdot}4H_2O$] were first dissolved into 150 mL of deionized water which was heated to ~60 °C and vigorously stirred. Dipotassium hydrogen phosphate ($K_2HPO_4{\cdot}3H_2O$), potassium hydroxide (KOH), and sodium fluoride (NaF) were added into another 150 mL of deionized water. After quickly mixing these two solutions, the as-obtained suspension or solution was sealed into an autoclave immediately and hydrothermally treated for 24 h at a given temperature. After cooling to room temperature, the white precipitate deposited in the bottom of the autoclave was collected and washed several times with deionized water and absolute ethanol, respectively.

The size and morphologies of the as-obtained samples were characterized by a field emission scanning electron microscope (FESEM, JSM-6700F, JEOL, Japan), a transmission electron microscope (TEM, H-700, Hitachi, Japan), and a high-resolution transmission electron microscope (HRTEM, JSM-2010, JEOL, Japan) operating at 200 kV. Energy-dispersive X-ray spectroscopy (EDX) was performed by an Oxford INCA energy system (Link-Inca, model 622, U.K.) with a Gatan 794 charge-coupled device. Phases were identified in an X-ray diffractometer (XRD, X′Pert, PANalytic, The Netherlands) with Cu Kα radiation (40 kV, 30 mA).

Results and Discussion

Structure and Morphologies. As shown in Figure 1, various morphologies, from fully developed prickly spheres, whisk brooms, nanorods, aggregated flowers, and long fibers to bundled nanoribbons, were synthesized by controlling the preparation parameters. The samples with these morphologies were sequentially analyzed by X-ray diffraction. By comparing with the standard cards (JCPDS no. 9-432 for HAp or no. 15-876 for fluorapatite, FAp), it was indicated that all the samples obtained are of apatite structure (hexagonal phase, space group $P6_3m$). The discrepancies of peak intensities resulted from the specified morphologies which affected the orientation of particles during preparation for XRD experiments.

Effect of Glutamic Acid. The effects of glutamic acid upon the formation and growth of apatite crystals were shown in Figure 2. Without the addition of glutamic acid, the resultant products were spheroidal nanocrystals with the average diameter of about ~80 nm, which were heavily aggregated as shown in Figure 2a. The addition of glutamic acid led to anisotropic growth of the resultant apatite (Figure 2b). With increasing the added amount of glutamic acid, slender apatite fibers with a less than 80 nm diameter were produced. These fibers radiated out from the centers and formed flowerlike aggregates with the overall size of 1−2 μm. Heavily aggregated nanocrystals with spheroidal morphology produced in the absence of glutamate ions and well-developed morphology of flowerlike apatite in the presence of glutamate ions indicated that the interaction between glutamate ions and precipitates could affect the transportation

(22) Mann, S.; Archibald, D. D.; Didymus, J. M.; Douglas, T.; Heywood, B. R.; Meldrum, F. C.; Reeves, N. J. *Science* **1993**, *261*, 1286.
(23) Tsortos, A.; Nancollas, G. H. *J. Colloid Interface Sci.* **2002**, *250*, 159.
(24) Flade, K.; Lau, C.; Mertig, M.; Pompe, W. *Chem. Mater.* **2001**, *13*, 3596.
(25) Wagner, C. C.; Baran, E. J. *J. Raman Spectrosc.* **2004**, *35*, 395.

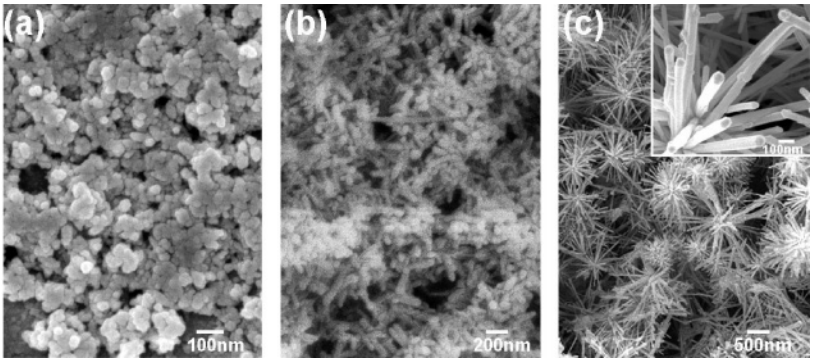

Figure 2. FESEM images of FHAp with varied glutamic acid addition on the basis of model reaction 1: (a) $C_G = 0$, (b) $C_G = 1.8$, and (c) $C_G = 3.6$. The pH values were adjusted to ~5.0 by adding HNO_3 or KOH.

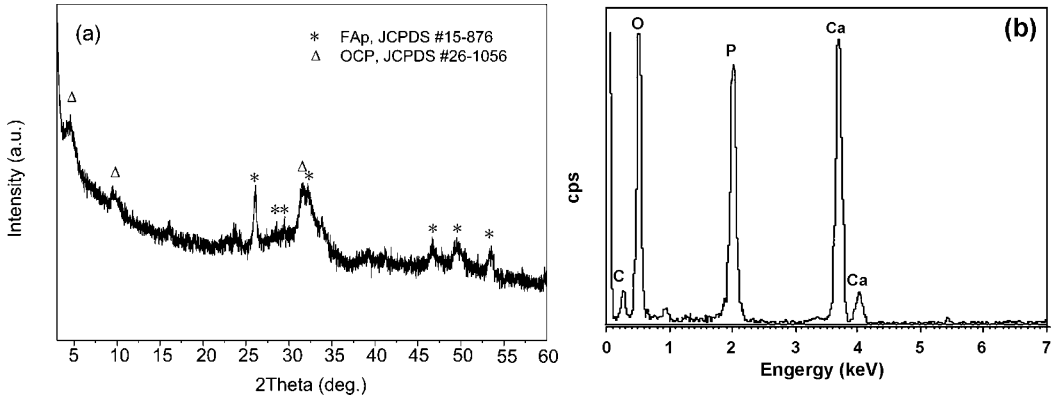

Figure 3. XRD pattern (a) and EDX spectrum (b) of the initial precipitates separated after 30 min of hydrothermal treatment of M1, $C_G = 3.6$. The pH was raised to ~5.0 by adding KOH.

of building units onto the crystal surface and finally shape the crystal growth along the specific direction.

To investigate how glutamate ions interacted with apatitic crystals and affected their growth, the sample was separated from the autoclaved suspension before the reaction was completed. The halfway separated sample showed the combined XRD patterns of apatite and octacalcium phosphate (OCP) in Figure 3a, and the Ca/P ratio was 1.45, which was less than 1.67 of stoichiometric hydroxyapatite and more than 1.33 of OCP (Figure 3b). Because the final product was FHAp, OCP was the intermediate phase and finally transformed into FHAp. Previous studies[19−20,26] showed that phosphoryn could be preferentially adsorbed on the (100) face of apatite and that polyglutamate could be absorbed on the hydrated layer of the OCP (100) face. As a result, these specific adsorptions greatly affected the morphology of OCP and the subsequent transformation into apatite. Thus, in our experiments, the interaction between glutamic acid and precipitated phases played an important role in the morphological development of final apatite crystals. These interactions had been summarized as hydrogen bonds, electrostatic attraction, calcium complex, and so forth.[22] Monma[27] and Mathew and Brown[28] proposed two structure models for the incorporation of dicarboxylate ions into OCP (the precursor of apatite), in which dicarboxylates replaced the HPO_4 groups in water layers of OCP. Marković et al.[29] investigated the formation of many OCP carboxylates besides glutamic acid-containing OCP and suggested that dicarboxylate ions replaced some HPO_4 groups and bridged two calcium ions diagonally throughout the space occupied by water molecules. Therefore, during the formation of apatite crystals through the precursor OCP, the interaction between calcium ions and carboxyl groups of glutamate ions would be one of the main factors which affected the morphological development.

Effect of Fluoride Ions. As shown in Figure 4, fluoride ions have a significant effect on the morphological development of apatite crystals. Under the experimental conditions of Figure 4a, fully developed apatite spheres were produced and these spheres were composed of delicate nanoneedles which were neatly arranged and bundled at one end. With the increase of fluoride concentration, the resultant apatite spheres were open and not fully developed (Figure 4b). Meanwhile, a little amount of whisk-broom-like crystal could be found as shown in the inset between parts a and b of Figure 4. To raise the fluoride concentration further, whisk brooms became the dominant morphology. But the handles of several whisk brooms intersected with each other and formed a dendritic morphology (Figure 4c,d). In other words, the first fractal growth, after nucleation, formed the dentritic stems; for example, the handles of the whisk brooms and the second splitting growth led to the whiskers of brooms. More concentrated fluoride solution decreased the number and length of whiskers in the ends of the brooms, and the

(26) Burke, E. M.; Guo, Y.; Colon, L.; Rahima, M.; Veis, A.; Nancollas, G. H. *Colloids Surf., B* **2000**, *17*, 49.
(27) Monma, H. *Bull. Chem. Soc. Jpn.* **1984**, *57*, 599.
(28) Mathew, M.; Brown, W. E. *Bull. Chem. Soc. Jpn.* **1987**, *60*, 1141.
(29) Marković, M.; Fowler, B. O.; Brown, W. E. *Chem. Mater.* **1993**, *5*, 1406.

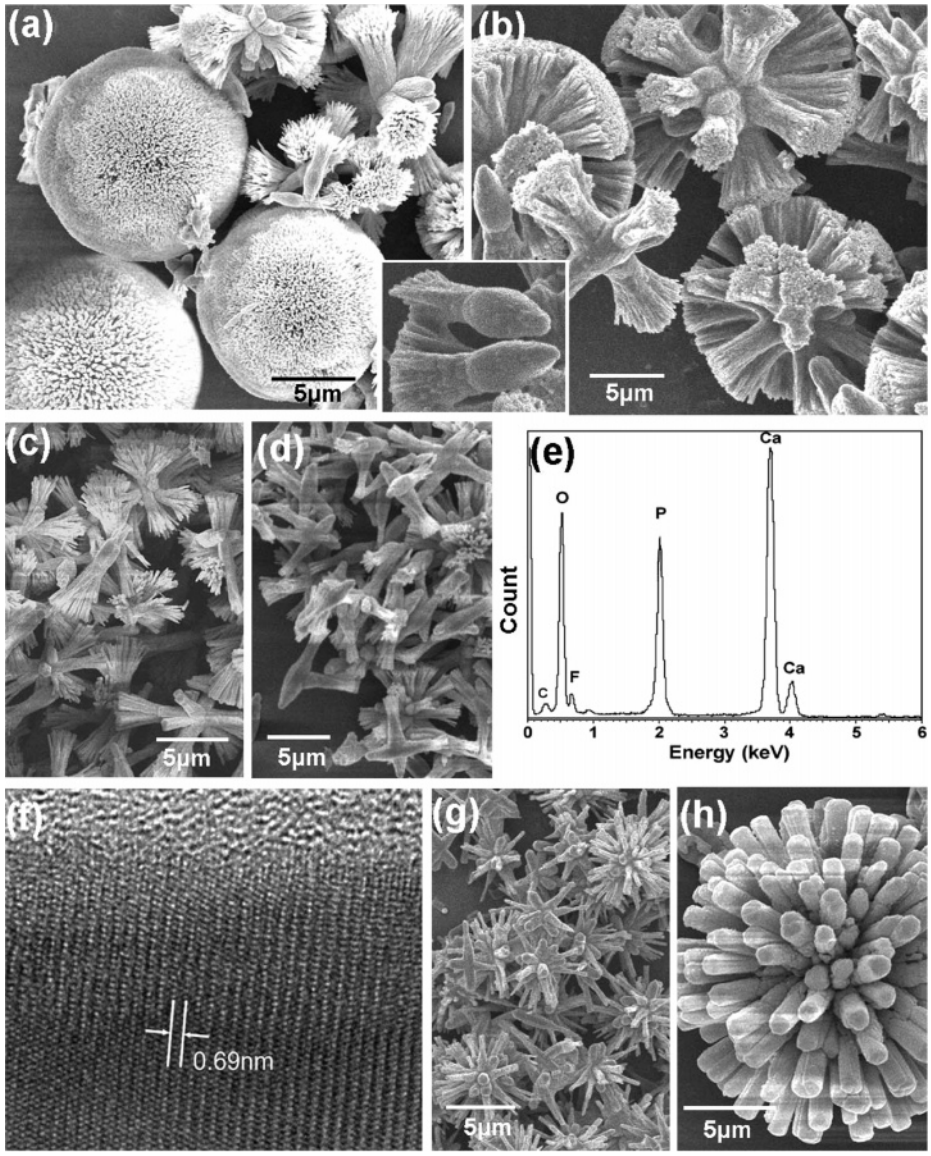

Figure 4. FESEM images of FHAp crystals obtained under varied fluoride addition on the basis of model reaction 2: (a) $C_{Ca}/C_P/C_F = 1.22:1.52:0.01$; (b) $C_F = 0.01$; (c) $C_F = 0.015$; (d−f) $C_F = 0.02$; (g) $C_F = 0.025$; and (h) $C_F = 0.1$.

round handle of the broom gradually evolved into a prismatic one. The EDX spectrum of the sample in Figure 4e showed that the sample contained 29.2 atom % Ca, 17.7 atom % P, and 2.8 atom % F, indicative of the formation of FHAp. As shown in Figure 4f, the HRTEM image of a whisker of the brooms obtained by ultrasonic treatment in a strong cell disruptor was taken along the long edge of a whisker. The 0.69 nm spacing of the atomic planes was consistent with that of the FAp (001) plane, suggesting that the whisker may be elongated along the [001] direction of the apatite crystal. When the concentration of fluoride increased further, as shown in Figure 4g, the whiskers of the brooms disappeared completely and prismatic rods with sharp tips radiated out from the center of the aggregates. In Figure 4h, the magnified image clearly showed that those sharp tips of prismatic rods grew into a symmetric hexagonal shape with clear edges, and the radial size of the rods also increased.

Analyzing various FESEM images led to the interpretation that fluoride greatly affected the fractal growth of apatite crystals. The formation of prickly spheres experienced the splitting growth twice. The increase of fluoride concentration promoted the formation of prismatic crystals. However, the occurrence of whisk-broom-like morphology is very interesting. It could be clearly seen in Figure 4 that this morphology is completely symmetric about the long axis, which is consistent with the hexagonal structure of apatite crystals; however, the symmetry of the hexagonal system should not inhibit the growth at one end of whisk-broom-like crystals and allow the splitting in the other end. This phenomenon differed from the dumbbell-like growth which was reported in a double-diffusion system.[30,31] To interpret the growth process, a schematic growth process was proposed as shown in Figure 5.

When the stock solutions were mixed (stage I), the initial nuclei were formed (stage II). If the supersaturation was relatively high, the newly formed nuclei were usually distinct both chemically and structurally from the final product,[32] which has been confirmed in Figure 3a,b. Brown proposed a mechanism for the crystal growth of biological apatites

(30) Kniep, R.; Busch, S. *Angew. Chem., Int. Ed. Engl.* **1996**, *35*, 2624.
(31) Busch, S.; Schwarz, U.; Kniep, R. *Adv. Funct. Mater.* **2003**, *13*, 189.
(32) Boskey, A. L.; Posner, A. S. *J. Phys. Chem.* **1976**, *80*, 40.

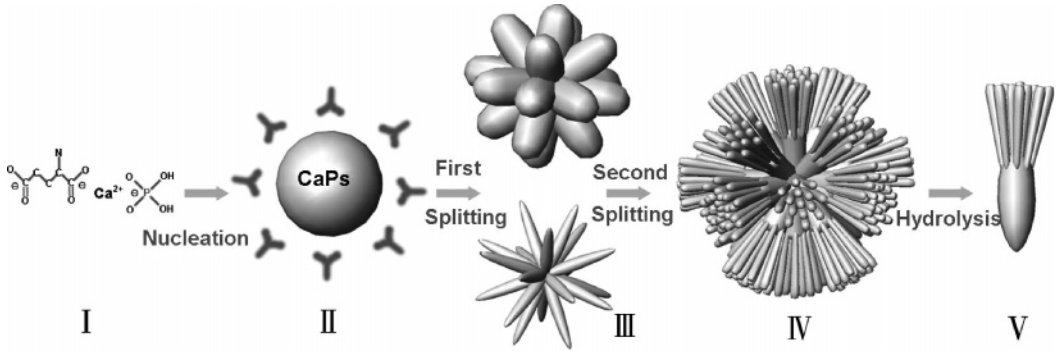

Figure 5. Schematic chart of the growth process.

that incorporated OCP as a transitory phase during the growth of apatite crystals.[33] The mechanism suggested that the nucleation of several-unit-cell thickness of OCP always preceded the growth of apatite crystals. The relative difference between the heterogeneous nucleating rate of OCP layers and the subsequent rate of hydrolyzing from OCP to HAp determined whether the crystal grows as OCP or HAp, and the difference would depend on conditions such as supersaturation, Ca/P ratio, pH, and temperature. The reason that the formation of HAp was preceded by an OCP layer is that the surface energy of HAp is greater than that of OCP[34] and the energy barrier for nucleating OCP is lower than that for HAp. Thus, the initial cores of prickly spheres which were formed quickly as a result of the high supersaturation were distinct from the apatite and would hydrolyze into the stable phase, FHAp, during prolonged hydrothermal treatment.

During the growing process of nucleated crystals, the hydrolysis of OCP to apatite led to the release of water along the *c* axis and splitting on the ends.[35] When the new layers were split (stage III), the preferential adsorption of glutamate ions on the {100} planes of a several-unit-cell OCP layer would retard the growth perpendicular to the planes and finally shaped the growth of newly branched crystals. The diffusion was blocked, and, thus, the hydrolysis of the initial cores (stage II → III) would slow because of the upgrowth of prickly shell on the core (stage III → IV) which was formed at the initial stage. So when the branched whiskers grew out (the second splitting), the hydrolysis of the internal cores (the first splitting) were not completed yet. The formation of whisk-broom-like morphology (stage V) was the result of the slow hydrolysis of cores after the second splitting as shown in Figure 5. The increased addition of fluoride ions relatively inhibited the second splitting growth and led to the morphologies in Figure 4g,h. Because fluoride was a strong mineralizing agent which accelerated the formation of FHAp at the stage of the first splitting growth, the absence of the second splitting growth led to the disappearance of whiskers in the tips of branched stems of Figure 4g,h as compared to the rayed whiskers in the end of brooms of Figure 4c,d.

Effect of KOH or pH. The pH value is of vital importance in the preparation of calcium phosphates including fluorine-substituted hydroxyapatite. Influence of pH values upon the morphological development of FHAp crystals are illustrated in Figure 6. When the pH value was relatively low, dentritic crystals after two splitting growths could be seen in Figure 6a. The stems formed after the first splitting growth radiated out from the center with decreasing radial size and produced sharp tips at the ends in the most cases. The tips of some stems grew out of delicate needlelike crystals through the second splitting growth. When the pH value was raised (Figure 6b), the number of branches owing to the first splitting growth increased significantly, and their radial size became slender in comparison with that in Figure 6a. The selected-area electron diffraction (SAED) pattern in Figure 6c confirmed that these flowerlike aggregates were apatite polycrystals. Higher pH led to the continued increase of the number of the first splitting growth. A large number of needlelike petals rayed out from the center and formed a dandelion-like morphology as shown in Figure 6d. When the experiment was performed at 160 °C, the resultant powder showed ultralong FHAp fibers with ~40 nm in diameter and several micrometers long. Although these fibers were entangled together, it could be found in Figure 6e that they grew out from one center.

The analysis of the EDX microprobe showed that the as-synthesized powder contained 28.3 atom % Ca, 17.1 atom % P, and 3.5 atom % F. The HRTEM image of a fiber in Figure 6g was taken along the long edge and showed that the spacing of atomic planes was 0.344 nm, which corresponded to that of the FAp (002) plane.[8] Because, in the XRD pattern of Figure 2e, the peak intensity of the (002) plane was weakened and that of the (300) plane increased, it indicated in conjunction with HRTEM analysis that the FHAp fiber was elongated along the *c*-axis direction.

Without the addition of fluoride, ultralong HAp nanoribbons were produced. Analyses of XRD and HRTEM confirmed that these nanoribbons were HAp instead of OCP because of the presence of characteristic spacing of {010} planes of 0.816 nm[36] and the absence of the strongest XRD reflection peak of OCP at 4.7°. The fast Fourier transformation analysis in the inset of Figure 6j, which was taken along the long edge of a ribbon, confirmed that the nanoribbon grew along the [001] direction. Because varied results of hydrolyzing of OCP to HAp were reported, including, mostly, needlelike,[19] notched,[35] platelike, and even struc-

(33) Brown, W. E. *Clin. Orthop.* **1966**, *44*, 205.
(34) Nelson, D. G. A.; Barry, J. C. *Anat. Rec.* **1989**, *224*, 265.
(35) Iijima, M.; Kamemizu, H.; Wakamatsu, N.; Goto, T.; Doi, Y.; Moriwaki, Y. *J. Cryst. Growth* **1997**, *181*, 70.
(36) Suvorova, E. I.; Buffat, P. A. *Eur. Cells Mater.* **2001**, *1*, 27.

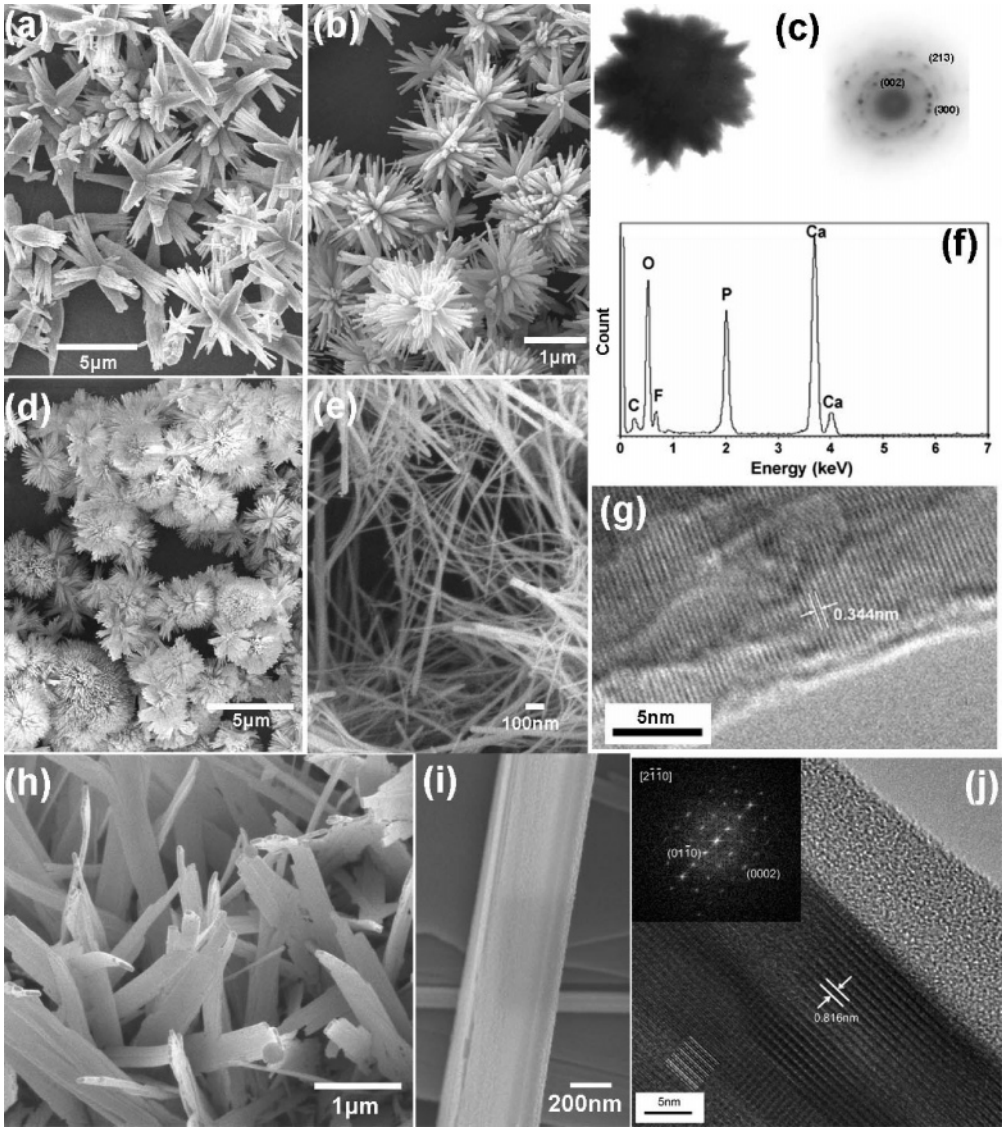

Figure 6. FESEM images, SAED pattern, and TEM image of FHAp crystals with varied KOH addition on the basis of model reaction 3: (a) $C_{OH} = 0.2$, pH = ~3.8; (b, c) $C_{OH} = 0.5$, pH = ~4.3; (d) $C_{OH} = 0.8$, pH = ~5.2; (e−g) $C_{OH}/T = 0.8{:}160$, pH = ~5.2; and (h) $C_F/C_{OH}/T = 0{:}1.04{:}160$, pH = ~5.8. HRTEM images of parts g and h were taken along the long edge of a fiber and ribbon, respectively.

tureless HAp[37] when directly hydrolyzing, the morphological development of such a uniform ribbonlike HAp nanocrystals in Figure 6h,i was related to the mediation of glutamic acid. The nanocrystals with ribbonlike morphology and apatitic structure led to the interpretation of two questions. First, nanoribbons were formed by two sequential processes. The building units in solutions were stacked onto the surface of nucleated crystals in the form of OCP structure, and the preferential adsorption of glutamate ions on {100} planes of the OCP layer mediated the growth rates along the *a* and *b* axes and led to the formation of ribbons instead of rods or needles. The precursor layer was very thin, possibly of several-unit-cell thickness. The hydrolysis process, gradually and closely, subsequently, converted the OCP layer into HAp. Thus, the morphology was like OCP crystals and the structure was of HAp. Second, the presence of fluoride led to the formation of fibrous crystals (Figure 6e) as compared to the ribbonlike crystals in Figure 6h,i. It further confirmed that fluoride accelerated the hydrolysis process, promoted the splitting along the water layer of OCP, and formed the morphology which was consistent with the hexagonal symmetry.

The morphological development through two splitting growths was related to the competition of two rates between the formation of the precursor and its transformation into the final product. Therefore, the adjustment of preparation parameters, such as the addition of fluoride, KOH, and Glu, may affect the morphological development by means of modulating this rate difference. Consequently, the morphologies of FHAp crystals could be controlled in this way.

Conclusions

Morphologies of FHAp crystals in microscale and nanoscale levels have been modulated from prickly spheres, whisk brooms, flowers, dandelions, and nanofibers to nanoribbons through adjusting the reaction conditions and adding glutamic acid. Plenty of experiments showed that FHAp crystals were formed, generally, through a fractal growth of two splittings. These two-splitting processes were related to the formation

(37) Graham, S.; Brown, P. W. *J. Cryst. Growth* **1996**, *165*, 106.

of precursor and its transformation into final products, which were affected by the interaction with glutamate ions and precipitates surfaces. Thus, through controlling the preparation parameters and adding glutamic acid, two-splitting processes were adjusted and then various morphologies were obtained. Prospectively speaking, this work not only obtained the morphology-controlled FHAp crystals but also fundamentally provided an effective and simple way to modulate inorganic material into well-defined morphologies with adding organic modifier.

Acknowledgment. This work was supported by National Natural Science Foundation of China (No. 20406023) and Chinese Academy of Sciences.

CM051357A